

# Electrical control of single hole spins in nanowire quantum dots

V. S. Pribiag<sup>1\*</sup>, S. Nadj-Perge<sup>1</sup>, S. M. Frolov<sup>1</sup>, J. W. G. van den Berg<sup>1</sup>, I. van Weperen<sup>1</sup>, S. R. Plissard<sup>2</sup>, E. P. A. M. Bakkers<sup>1,2</sup> and L. P. Kouwenhoven<sup>1\*</sup>

**The development of viable quantum computation devices will require the ability to preserve the coherence of quantum bits (qubits)<sup>1</sup>. Single electron spins in semiconductor quantum dots are a versatile platform for quantum information processing, but controlling decoherence remains a considerable challenge<sup>1–4</sup>. Hole spins in III–V semiconductors have unique properties, such as a strong spin–orbit interaction and weak coupling to nuclear spins, and therefore, have the potential for enhanced spin control<sup>5–8</sup> and longer coherence times<sup>8–12</sup>. A weaker hyperfine interaction has previously been reported in self-assembled quantum dots using quantum optics techniques<sup>10–12</sup>, but the development of hole–spin-based electronic devices in conventional III–V heterostructures has been limited by fabrication challenges<sup>13</sup>. Here, we show that gate-tunable hole quantum dots can be formed in InSb nanowires and used to demonstrate Pauli spin blockade and electrical control of single hole spins. The devices are fully tunable between hole and electron quantum dots, which allows the hyperfine interaction strengths, *g*-factors and spin blockade anisotropies to be compared directly in the two regimes.**

Electron spins in III–V semiconductors undergo rapid decoherence because of strong hyperfine coupling to the surrounding nuclear spin bath<sup>2–4</sup>. In contrast, the contact hyperfine interaction for hole spins is predicted to vanish due to the *p*-orbital symmetry of their Bloch wavefunction, leaving only the weaker dipole–dipole coupling<sup>9</sup>. However, conventional *p*-doped quantum wells do not provide the required level of stability and tunability to allow hole spins in gate-defined quantum dots to be investigated<sup>13</sup>. An alternative approach is to use an undoped structure with a small enough bandgap that the hole transport regime can be accessed simply by means of gate tuning. InSb is an excellent candidate for this because it has the smallest bandgap in the III–V family of semiconductors<sup>14</sup>. Defect-free InSb nanowires can be grown using bottom-up methods, which offer precise control over crystal structure and electronic properties<sup>15–17</sup>. As well as their small bandgap, these nanowires are of interest for quantum devices because of the presence of strong spin–orbit coupling and large *g*-factors, which has allowed signatures of Majorana fermions to be detected in the solid state<sup>18</sup> and also fast all-electrical spin control<sup>14,19</sup>.

To illustrate tuning between electron and hole transport, we first use a basic device consisting of an InSb nanowire placed above a doped silicon backgate (Fig. 1). For positive backgate voltages  $V_{BG}$ , the Fermi level is tuned into the conduction band, resulting in a source–drain current of  $\sim 1 \mu\text{A}$  due to accumulation of electrons. The current is suppressed as  $V_{BG}$  is decreased to around  $-5 \text{ V}$  and the Fermi level enters the bandgap. At around  $-14 \text{ V}$ , current is then restored due to accumulation of holes<sup>16</sup>. We rely

on this basic tunability for defining hole quantum dots in the nanowires.

To confine holes to quantum dots, we fabricated devices with five narrow gates that allow local control of the Fermi level<sup>15,19</sup> (Fig. 2a). Taking advantage of the small bandgap of InSb, a hole quantum dot can be formed by inducing holes into a short section of the nanowire using a single fine gate (gate 2). The rest of the nanowire remains *n*-type, as shown schematically in Fig. 2b. Strong band bending above gate 2 forms an attractive potential well for holes between two *p*–*n* junctions<sup>20</sup>. A transition from an entirely *n*-type wire to such an npn quantum dot is displayed in Fig. 2c for device d1. As the gate 2 voltage  $V_G$  is decreased from around zero, the current through the *n*-type device is suppressed by the formation of a tunnel barrier above the gate (see right schematic in Fig. 2c). As  $V_G$  is decreased further, we observe Coulomb diamonds, indicating that transport in this region is mediated by the first few hole states of the quantum dot (see left schematic in Fig. 2c). Interestingly, the 0-hole (0h) Coulomb diamond crosses the boundary of the electron transport regime at a bias of  $\sim 90 \text{ mV}$ , which corresponds to less than half the value of the bandgap for our InSb nanowires ( $\sim 200 \text{ meV}$ , Supplementary Fig. S1). This suggests that at larger bias (or at less negative  $V_G$ ), electrons tunnel more efficiently

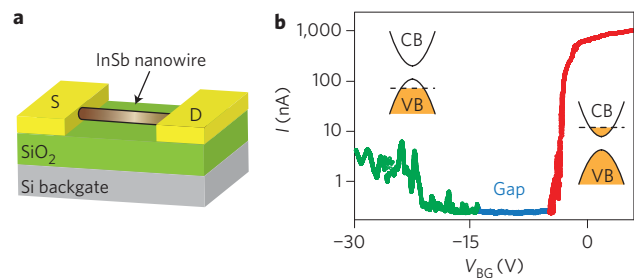


**Figure 1 | Ambipolar transport in an InSb nanowire.** **a**, Schematic of a device used to demonstrate ambipolar transport in InSb nanowires. **b**, Current through an InSb nanowire as a function of voltage  $V_{BG}$  applied to the silicon backgate, for a device as shown in **a** (source–drain bias  $V_{SD} = 10 \text{ mV}$ ). The nanowire is separated from the backgate by  $285 \text{ nm}$  of  $\text{SiO}_2$ , and the spacing between the source and drain Ti/Au contacts is  $\sim 300 \text{ nm}$ . Right (left) insets: when the Fermi level is tuned to the conduction (valence) band, current transport in the nanowire is mediated by electrons (holes). Hole conductance is typically one to two orders of magnitude lower than electron conductance. This could indicate reduced transparency of the nanowire–metal contact interface for holes<sup>16</sup> or lower hole mobility<sup>14</sup>. The measured bandgap is  $\sim 0.2 \text{ eV}$ , in agreement with the bulk value for InSb (ref 14; Supplementary Fig. S1).

<sup>1</sup>Kavli Institute of Nanoscience, Delft University of Technology, 2600 GA Delft, The Netherlands, <sup>2</sup>Department of Applied Physics, Eindhoven University of Technology, 5600 MB Eindhoven, The Netherlands. \*e-mail: v.s.pribiag@tudelft.nl; l.p.kouwenhoven@tudelft.nl

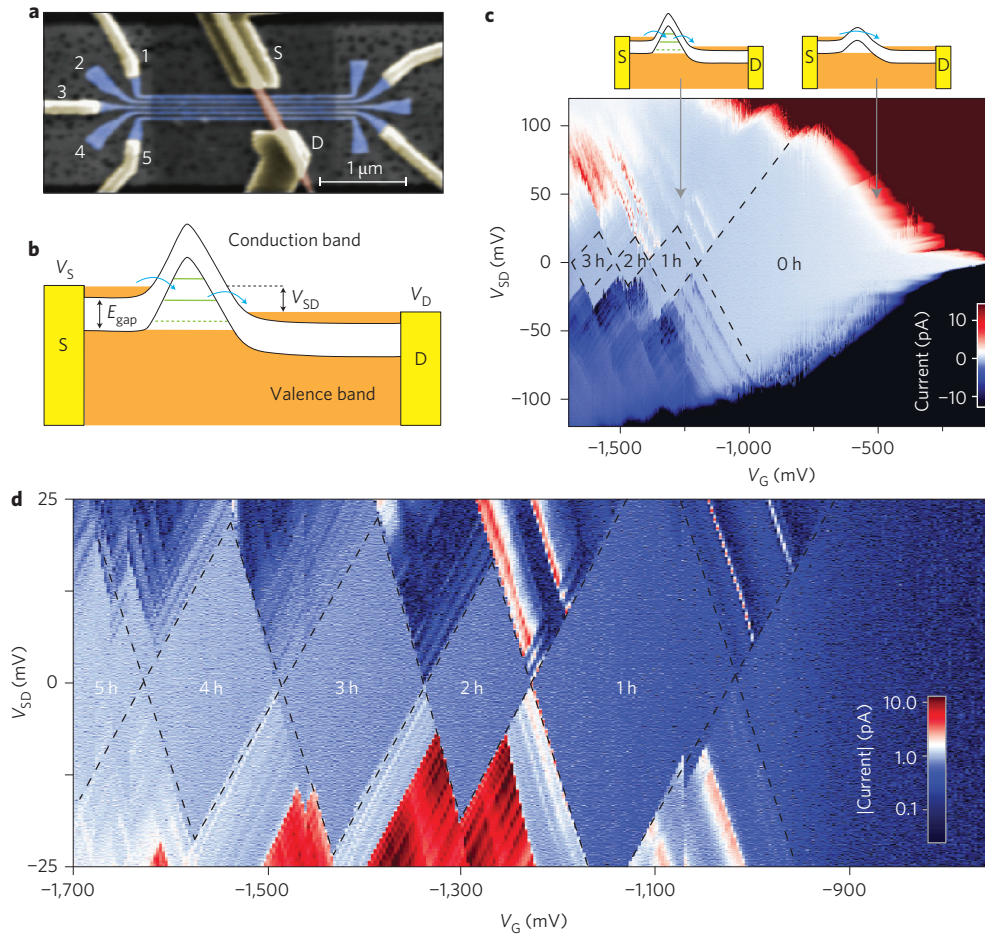


**Figure 2 | Gate tuning between electron transport and hole quantum dot.** **a**, Scanning electron microscopy image of a typical gated InSb nanowire device used for studying quantum dots. The gate widths and intergate spacing are  $\sim 30$  nm; the source and drain contacts are made of Ti/Al. A wider metallic gate is used to control the charge density in the nanowire segments between the narrow gates and the source and drain electrodes. The wide gate is separated from the narrow gates by a 50 nm layer of  $\text{Si}_3\text{N}_4$ . The fine gates are covered by an additional 25 nm layer of  $\text{Si}_3\text{N}_4$ . **b**, Schematic of band diagram showing a gate-defined hole quantum dot. Tunnelling between the dot and the n-type leads occurs via p-n junctions. **c**, Charge stability diagram (device d1) of a device as in **a**, shown as a function of source-drain bias  $V_{SD}$  and plunger gate voltage  $V_G$ . For less negative  $V_G$ , the nanowire is n-type and current is carried by electrons. For more negative  $V_G$ , transport is suppressed due to the bandgap of the nanowire. For even more negative  $V_G$ , a hole quantum dot is formed above the plunger gate. In this regime a finite transport current is observed as a result of tunnelling via discrete hole states in the dot. **d**, Hole Coulomb diamonds for device d1 (the dot potential is tuned slightly differently than in **c**). The fluctuating diamond sizes and the absence of any further transitions to the right of the diamond labelled '0 h' are consistent with the few-hole regime. However, unambiguous identification of the number of holes would require a charge sensor. From the size of the Coulomb diamonds we estimate that charging energies  $E_c$  of single holes are on the scale of 20 meV and orbital energies  $E_{orb}$  are between 3 and 8 meV.

directly through the conduction band barrier than through the two p-n junctions adjacent to the quantum dot (see tunnelling schematics in Fig. 2c). A more detailed view of the first five hole diamonds (Fig. 2d) shows distinct resonances in the quantum dot transport regime. These resonances are typical signatures of quantum dot excited states<sup>3</sup>, but can also originate from singularities in the density of states in the leads<sup>21</sup>. We find that for our hole quantum dots the two mechanisms can be distinguished based on their different magnetic field dependence (Supplementary Fig. S3).

To investigate spin-dependent transport for holes we rely on double quantum dots tuned to the Pauli spin blockade<sup>3</sup> regime. Pauli spin blockade provides a reliable means to initialize and read out spin states in a double dot, and has been studied extensively for electrons<sup>3</sup>. Whenever the spins of unpaired electrons on separate dots form a triplet state, tunnelling between the dots is suppressed, because the final state with the two electrons on the same orbital must be a singlet. Holes in III-V semiconductors

differ in many respects from electrons, being characterized by different effective masses and strong coupling of spin to *p* orbitals<sup>22</sup>. To form hole double quantum dots we use either gates 2 and 4 (achieving weak interdot coupling) or gates 2 and 3 (achieving strong interdot coupling) to confine holes in adjacent segments of the nanowire (Fig. 3a). Just as in the case of single dots, tunnelling between a double dot and the leads occurs through p-n junctions. The two gates can be used to tune between an entirely n-type wire and an nppn double dot, as shown in the inset of Fig. 3b. More generally, the devices can be fully tuned between hole double dots and electron double dots by varying the voltages on all five fine gates. The electron regime has been studied in detail in ref. 19 using device d2. The main panel of Fig. 3b shows a zoomed-in view of the charge stability diagram of a few-hole double dot for device d2. Triple-point bias triangles separate regions where the number of holes in each dot is fixed by Coulomb blockade. Alternating spacing between the triple point transitions, together with the absence of lower charge states in

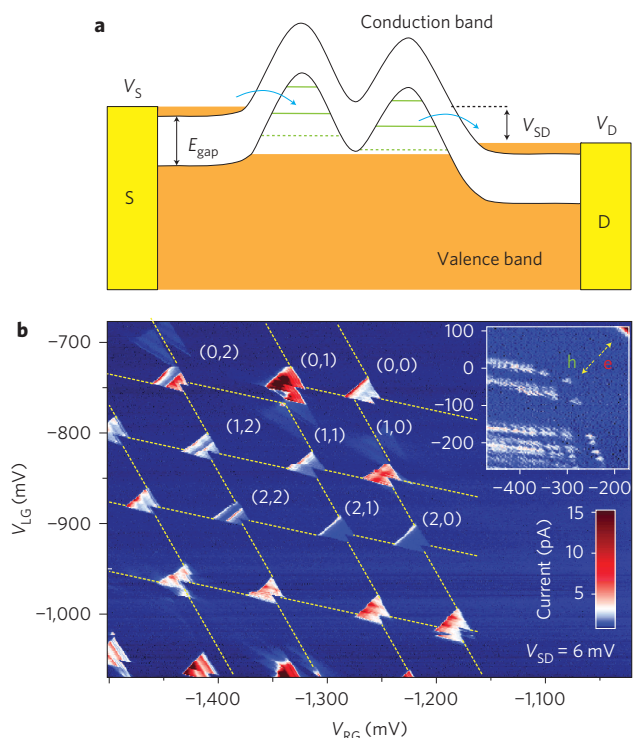


**Figure 3 | Gate-defined few-hole double quantum dot.** **a**, Schematic band diagram showing a hole double quantum dot and n-type leads. Tunnelling onto and off the double dot occurs via p-n junctions. **b**, Charge stability diagram of a hole double quantum dot as a function of the left and right plunger gate voltages ( $V_{LG}$  and  $V_{RG}$ ) (device d2, first cooldown). The larger, dimmer triangles are attributed to an additional quantum dot located in series to the right of the hole double dot and strongly coupled to the drain reservoir (Supplementary Section S2). We estimate the size of the dots to be  $\sim 15$  nm from  $I_{dot} \sim \hbar/\sqrt{E_{orb}m_{hole}}$ . Inset: stability diagram over a larger area of gate space (device d1,  $V_{SD} = 12$  mV), showing the transition from electron transport (upper-right corner) to the hole double dot regime (lower-left region).

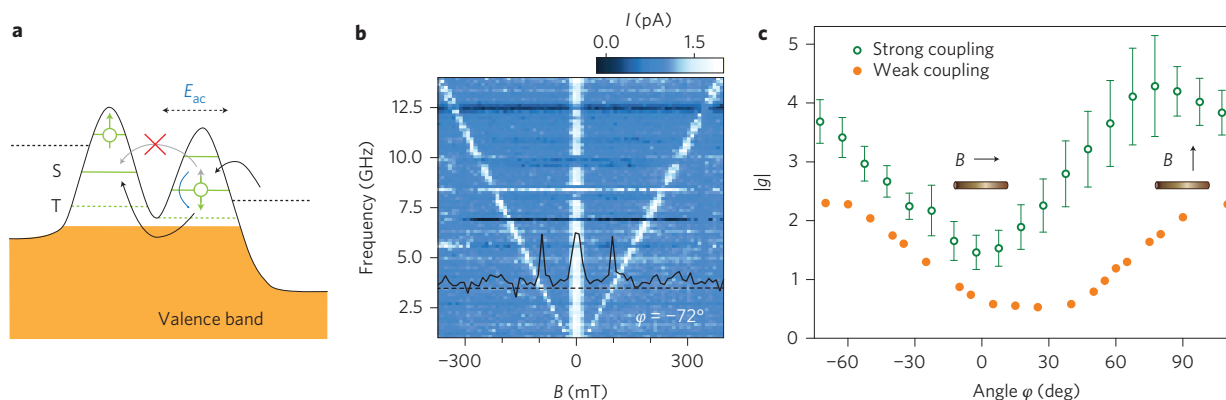
the stability diagram, suggest that the double dot occupancy can be controlled down to the last hole (however, charge sensing would be necessary to unambiguously determine the occupancy). Charging energies  $E_c$  are  $\sim 20$  meV, while the orbital separation  $E_{orb}$ ,

extracted from excited state measurements on the (1,0) state, is  $\sim 8$  meV, in agreement with the single-dot values. It is useful to note that the ratio  $E_c^2/E_{orb}$  is proportional to the effective mass, but is independent of the quantum dot size in a first approximation<sup>3</sup>. By comparing the value of  $E_c^2/E_{orb}$  obtained here for holes with the value for electrons<sup>19</sup>, we find that the effective hole mass in our quantum dots is comparable to that of electrons, in agreement with expectations for light holes (LHs) in InSb ( $m_{LH} \approx 0.015 m_e$ ,  $m_e^* \approx 0.014 m_e$ ), and more than an order of magnitude lighter than the heavy hole (HH) mass ( $m_{HH} \approx 0.43 m_e$ )<sup>14</sup>. This suggests that the states in our double dots are predominantly LH-like. Moreover, LHs are also likely to dominate charge transport due to the angular momentum mismatch between heavy holes ( $J_z = 3/2$ ) and spin-1/2 electrons in the leads.

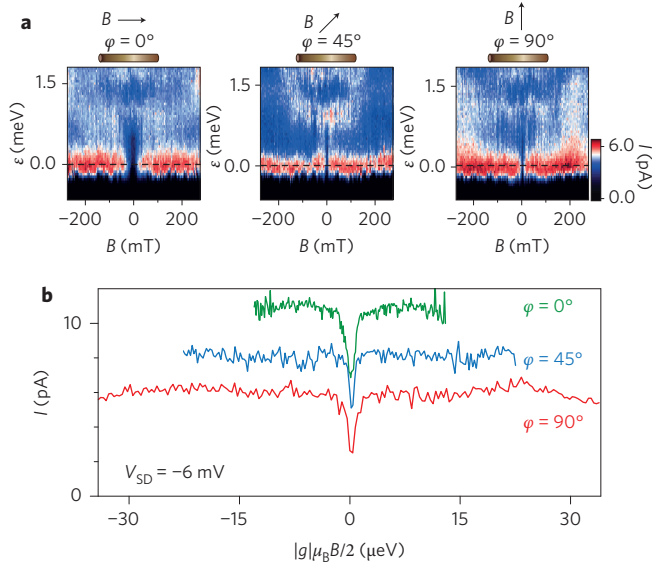
Spin blockade is lifted by any process that mixes triplets and singlets, such as single-spin rotations. In the presence of strong spin-orbit interaction (SOI), spin rotations can be induced by a microwave-frequency electric field applied with one of the plunger gates. This electric dipole spin resonance (EDSR)<sup>23,24</sup> mechanism is expected to drive single hole spin rotations whenever the frequency  $f_0$  of the applied electric field matches the Zeeman energy of the hole spin ( $f_0 = g\mu_B B/h$ , where  $g$  is the Landé  $g$ -factor,  $\mu_B$  is the Bohr magneton,  $B$  is the applied static magnetic field, and  $h$  is Planck's constant). Lifting of the spin blockade by EDSR allows holes to tunnel between the two dots (Fig. 4a).

Figure 4b shows the V-shaped resonance, mapped out by measuring the double-dot current as a function of  $f_0$  and  $B$ . In addition to the EDSR lines, we also observe a current peak near  $B = 0$ . By analogy with the case of electrons, we attribute this feature to the hyperfine interaction (Supplementary Fig. S4 shows more details about hole spin blockade in the case of weak interdot coupling)<sup>3,25-27</sup>. From the peak width we estimate the root mean squared (r.m.s.) fluctuations of the hyperfine interaction for holes,  $E_{N,h} \approx 0.8 \mu eV$ , using the standard method described in ref. 28 (Supplementary Section S2). Thanks to the extensive tunability, we are able to perform the same analysis on data from the electron double dot regime of the same device, and obtain  $E_{N,e} \approx 2 \mu eV$ . Taking into account the electron and hole dot volumes, we estimate the ratio of the hyperfine coupling strength for electrons to that for holes:  $A_e/A_h \approx 7$ . This value is close to the values obtained using optical techniques on self-assembled dots<sup>29</sup>.

The hole  $g$ -factor extracted from the EDSR spectra (Fig. 4c) shows remarkable differences from the electron  $g$ -factor<sup>19</sup> in both magnitude and anisotropy. The magnitude ranges between  $\sim 0.5$



**Figure 4 | Electric-dipole spin resonance and hole  $g$ -factor anisotropy.** **a**, Interdot tunnelling is suppressed by spin blockade whenever unpaired holes in each dot form a triplet state (T). A microwave-frequency electric field of amplitude  $E_{ac}$  applied to the right plunger gate induces spin rotation to a singlet (S) by means of EDSR, lifting the spin blockade. **b**, EDSR for weak interdot coupling (device d2, second cooldown). The line cut is at  $f = 3.4$  GHz. In addition to the EDSR resonances, we observe a lifting of the spin blockade near  $B = 0$ , attributed to the hyperfine interaction. **c**, Anisotropy of the hole  $g$ -factor extracted from EDSR measurements for different angles  $\phi$  between the applied magnetic field  $B$  and the nanowire axis in the plane of the sample surface. Weak coupling  $g$ -factor data is from the second cooldown of device d2 and strong coupling data from the third cooldown of the same device.



**Figure 5 | Hole spin blockade for strong interdot coupling.** **a**, Double-dot current versus detuning  $\varepsilon$  and magnetic field  $B$  in the strong-coupling regime for three different angles (device d2, third cooldown,  $V_{SD} = -6$  mV). Spin blockade is observed as a dip near  $B = 0$ . **b**, Cuts along the dotted lines at  $\varepsilon = 0$  in **a**. The applied magnetic field is scaled by the effective  $g$ -factors at each angle (see Fig. 4). For clarity, the data for  $\varphi = 45^\circ$  and  $\varphi = 0^\circ$  are offset vertically by 2.5 pA and 5.0 pA, respectively. Offsets of several mT due to the magnet were subtracted from the data in **a** and **b**.

and  $\sim 4$  for holes, far less than the typical range of  $\sim 35$  to  $\sim 45$  for electrons. The hole  $g$ -factor is expected to be a strong function of the nanowire subband<sup>30</sup>, ranging between  $\sim 0$  and several times the value of the bulk hole  $g$ -factor  $\kappa$  ( $\kappa = 15.6$  for InSb<sup>22</sup>). The small  $g$ -factor values and strong anisotropy we observe could therefore be a consequence of hole mixing<sup>25,26</sup> due to confinement by the quantum dot potential. An important point, evident when comparing the data for the strong and the weak coupling regimes, is that both the magnitude and the anisotropy of the  $g$ -factor are sensitive to the details of the quantum dot potential. This strong dependence on gate voltages indicates that gate-induced  $g$ -tensor modulation<sup>31</sup> contributes to the EDSR mechanism, in addition to direct driving by the SOI.

Measurements of spin blockade in the strong coupling regime highlight a further difference between electron and hole spins. In this coupling regime, hole spin blockade is lifted at finite  $B$ , leading to a dip around  $B = 0$  (Fig. 5 and Supplementary Fig. S6). For electrons, the lifting of spin blockade at finite  $B$  is due to mixing of blocked and unblocked spin states by the SOI<sup>19,26,27</sup>. A dramatic signature of this mechanism is strong anisotropy of the spin blockade as a function of the angle between  $B$  and the nanowire<sup>19,27</sup>. However, in contrast to the case of electrons, here we find that hole spin blockade is almost isotropic at zero detuning and only weakly anisotropic at finite detuning (Fig. 5b and Supplementary Fig. S6). It is important to note that the expected anisotropy is not related to the shape or size of the quantum dot. Instead, it originates from the fixed direction of the Rashba spin-orbit field, as determined by the sample geometry. The absence of spin blockade anisotropy for holes is thus intriguing given the anisotropic  $p$ -orbital symmetry of hole Bloch wavefunctions<sup>22</sup>, especially given that the device geometry is identical to that used for electrons in ref. 19. This suggests that either spin blockade for holes is not described by the same model as for electrons<sup>27</sup> or the dominant SOI for holes is not of the Rashba type.

In summary, our work establishes InSb nanowires as a promising platform for tunable hole quantum dots and demonstrates the

importance of the SOI for controlling single hole spins. This provides an avenue for testing the potential for faster and more coherent spin manipulation using holes. Furthermore, gated InSb nanowires may be a viable platform for Majorana fermion detection using holes<sup>32</sup>, with the observed  $g$ -factors being sufficiently large to exceed the required  $g > 2$  threshold<sup>33</sup>. Finally, the ability to confine single holes and single electrons in the same nanostructure opens the way for unique applications, such as controlled exchange between hole and electron spins and coupling of distant spins via photons, all achievable in III-V semiconductor nanowires using established quantum transport and quantum optics techniques.

## Methods

Zincblende InSb nanowires ( $\sim 100$  nm diameter and 2–3  $\mu\text{m}$  long) were grown using metal-organic vapour phase epitaxy with the [111]-axis oriented along the growth direction<sup>17</sup>. Nanowires were mechanically transferred in air from the growth substrate to a second substrate with pre-patterned gate structures. Contacts were made to selected nanowires. Quantum dot measurements were performed in a He<sup>3</sup> refrigerator with a base temperature of 300 mK, equipped with a two-axis vector magnet. Few-hole quantum dots and spin blockade were observed in two different devices and EDSR was measured on one device for three different cooldowns.

Received 6 June 2012; accepted 9 January 2013;  
published online 17 February 2013

## References

- Loss, D. & DiVincenzo, D. P. Quantum computation with quantum dots. *Phys. Rev. A* **57**, 120–126 (1998).
- Petta, J. R. *et al.* Coherent manipulation of coupled electron spins in semiconductor quantum dots. *Science* **309**, 2180–2184 (2005).
- Hanson, R., Petta, J. R., Tarucha, S. & Vandersypen, L. M. K. Spins in few-electron quantum dots. *Rev. Mod. Phys.* **79**, 1217–1265 (2007).
- Nadj-Perge, S., Frolov, S. M., Bakkers, E. P. A. M. & Kouwenhoven, L. P. Spin-orbit qubit in a semiconductor nanowire. *Nature* **468**, 1084–1087 (2010).
- Manaselyan, A. & Chakraborty, T. Enhanced Rashba effect for hole states in a quantum dot. *Europhys. Lett.* **88**, 17003–17007 (2009).
- Katsaros, G. *et al.* Hybrid superconductor-semiconductor devices made from self-assembled SiGe nanocrystals on silicon. *Nature Nanotech.* **5**, 458–464 (2010).
- Kloeffel, C., Trif, M. & Loss, D. Strong spin-orbit interaction and helical hole states in Ge/Si nanowires. *Phys. Rev. B* **84**, 195314 (2011).
- Hu, Y. J., Kuemmeth, F., Lieber, C. M. & Marcus, C. M. Hole spin relaxation in Ge-Si core-shell nanowire qubits. *Nature Nanotech.* **7**, 47–50 (2012).
- Fischer, J., Coish, W. A., Bulaev, D. V. & Loss, D. Spin decoherence of a heavy hole coupled to nuclear spins in a quantum dot. *Phys. Rev. B* **78**, 155329 (2008).
- Brunner, D. *et al.* A coherent single-hole spin in a semiconductor. *Science* **325**, 70–72 (2009).
- De Greve, K. *et al.* Ultrafast coherent control and suppressed nuclear feedback of a single quantum dot hole qubit. *Nature Phys.* **7**, 872–878 (2011).
- Greilich, A., Carter, S. G., Kim, D., Bracker, A. S. & Gammon, D. Optical control of one and two hole spins in interacting quantum dots. *Nature Photon.* **5**, 702–708 (2011).
- Grbic, B. *et al.* Hole transport in p-type GaAs quantum dots and point contacts. *AIP Conf. Proc.* **893**, 777–778 (2007).
- Madelung, O. *Semiconductors: Data Handbook* 3rd edn (Springer, 2004).
- Nilsson, H. A. *et al.* Giant, level-dependent  $g$  factors in InSb nanowire quantum dots. *Nano Lett.* **9**, 3151–3156 (2009).
- Nilsson, H. A. *et al.* InSb nanowire field-effect transistors and quantum-dot devices. *IEEE J. Sel. Top. Quant.* **17**, 907–914 (2011).
- Plissard, S. R. *et al.* From InSb nanowires to nanocubes: looking for the sweet spot. *Nano Lett.* **12**, 1794–1798 (2012).
- Mourik, V. *et al.* Signatures of Majorana fermions in hybrid superconductor-semiconductor nanowire devices. *Science* **336**, 1003–1007 (2012).
- Nadj-Perge, S. *et al.* Spectroscopy of spin-orbit quantum bits in indium antimonide nanowires. *Phys. Rev. Lett.* **108**, 166801 (2012).
- Steele, G. A., Gotz, G. & Kouwenhoven, L. P. Tunable few-electron double quantum dots and Klein tunnelling in ultraclean carbon nanotubes. *Nature Nanotech.* **4**, 363–367 (2009).
- Escott, C. C., Zwanenburg, F. A. & Morello, A. Resonant tunnelling features in quantum dots. *Nanotechnology* **21**, 274018 (2010).
- Winkler, R. *Spin-Orbit Coupling Effects in Two-Dimensional Electron and Hole Systems* (Springer, 2003).
- Rashba, E. I. Theory of electric dipole spin resonance in quantum dots: mean field theory with Gaussian fluctuations and beyond. *Phys. Rev. B* **78**, 195302 (2008).

24. Bulaev, D. V. & Loss, D. Electric dipole spin resonance for heavy holes in quantum dots. *Phys. Rev. Lett.* **98**, 097202 (2007).
25. Churchill, H. O. H. *et al.* Electron–nuclear interaction in  $^{13}\text{C}$  nanotube double quantum dots. *Nature Phys.* **5**, 321–326 (2009).
26. Nadj-Perge, S. *et al.* Disentangling the effects of spin–orbit and hyperfine interactions on spin blockade. *Phys. Rev. B* **81**, 201305(R) (2010).
27. Danon, J. & Nazarov, Y. V. Pauli spin blockade in the presence of strong spin–orbit coupling. *Phys. Rev. B* **80**, 041301(R) (2009).
28. Koppens, F. H. L. *et al.* Control and detection of singlet–triplet mixing in a random nuclear field. *Science* **309**, 1346–1350 (2005).
29. Chekhovich, E. A., Krysa, A. B., Skolnick, M. S. & Tartakovskii, A. I. Direct measurement of the hole–nuclear spin interaction in single InP/GaInP quantum dots using photoluminescence spectroscopy. *Phys. Rev. Lett.* **106**, 027402 (2011).
30. Csontos, D., Brusheim, P., Zulicke, U. & Xu, H. Q. Spin-3/2 physics of semiconductor hole nanowires: Valence-band mixing and tunable interplay between bulk-material and orbital bound-state spin splittings. *Phys. Rev. B* **79**, 155323 (2009).
31. Kato, Y. *et al.* Gigahertz electron spin manipulation using voltage-controlled  $g$ -tensor modulation. *Science* **299**, 1201–1204 (2003).
32. Mao, L., Gong, M., Dumitrescu, E., Tewari, S. & Zhang, C. Hole-doped semiconductor nanowire on top of an  $s$ -wave superconductor: a new and experimentally accessible system for Majorana fermions. *Phys. Rev. Lett.* **108**, 177001 (2012).
33. Lutchyn, R. M., Sau, J. D. & Das Sarma, S. Majorana fermions and a topological phase transition in semiconductor–superconductor heterostructures. *Phys. Rev. Lett.* **105**, 077001 (2010).

### Acknowledgements

The authors thank L.M.K. Vandersypen and G. Bauer for helpful discussions and comments. This work has been supported by the Dutch Organization for Fundamental Research on Matter (FOM), the Netherlands Organization for Scientific Research (NWO) and the European Research Council (ERC). V.S.P. acknowledges support from NWO through a VENI grant.

### Author contributions

V.S.P., S.N., S.M.F., J.W.G.B. and I.W. performed the measurements. V.S.P., S.N., S.M.F. and J.W.G.B. analysed the data. V.S.P., S.N. and J.W.G.B. fabricated the devices. S.R.P. and E.P.A.M.B. provided the nanowires. L.P.K. supervised the project. All authors contributed to writing the manuscript.

### Additional information

Supplementary information is available in the [online version](#) of the paper. Reprints and permissions information is available online at [www.nature.com/reprints](http://www.nature.com/reprints). Correspondence and requests for materials should be addressed to V.S.P. and L.P.K.

### Competing financial interests

The authors declare no competing financial interests.